Nanostructured Organic Layers via Polymer Demixing for Interface-Enhanced Photovoltaic Cells

Fernando A. Castro,[†,‡] Hadjar Benmansour,[†] Carlos F. O. Graeff,[§] Frank Nüesch,[†] Eduard Tutis,[||] and Roland Hany*[,†]

Empa, Swiss Federal Laboratories for Materials Testing and Research, Laboratory for Functional Polymers, Überlandstr. 129, CH-8600 Dübendorf, Switzerland, Departamento de Física e Matemática, Faculdade de Filosofia, Ciências e Letras de Ribeirão Preto, Universidade de São Paulo, Av. Bandeirantes 3900, 14040-901, Ribeirão Preto, SP, Brazil, Departamento de Física, Faculdade de Ciências, UNESP, Av. Luiz Edmundo Carrijo Coube 14-01, 17033-360 Bauru, Brazil, and Institute of Physics, P.O. Box 304, HR-1000 Zagreb, Croatia

Received July 17, 2006. Revised Manuscript Received August 31, 2006

Significant progress is being made in the photovoltaic energy conversion using organic semiconducting materials. One of the focuses of attention is the morphology of the donor−acceptor heterojunction at the nanometer scale, to ensure efficient charge generation and loss-free charge transport at the same time. Here, we present a method for the controlled, sequential design of a bilayer polymer cell architecture that consists of a large interface area with connecting paths to the respective electrodes for both materials. We used the surface-directed demixing of a donor conjugated/guest polymer blend during spin coating to produce a nanostructured interface, which was, after removal of the guest with a selective solvent, covered with an acceptor layer. With use of a donor poly(*p*-phenylenevinylene) derivative and the acceptor C_{60} fullerene, this resulted in much-improved device performance, with external power efficiencies more than 3 times higher than those reported for that particular material combination so far.

Introduction

The emerging field of organic semiconductor materials stimulates new approaches to the production of efficient low-cost photovoltaic devices.[1−4] State-of-the-art organic solar cells are commonly fabricated from a combination of an electron-donor and -acceptor material with suitable redox energy levels, sandwiched as a thin (≤200 nm) film between metallic electrodes.[5,6] Photoexcitation of the organic material leads to an exciton, or a bound electron−hole pair. The exciton is then dissociated into free carriers in a strong electric field or at the donor−acceptor interface.[7,8] Subsequently, electrons and holes are transported via drift and diffusion processes to the electrodes, where they are collected, giving rise to an electric current.[3,9] The yield of charge generation and charge collection determine the device efficiency. The small (∼10 nm) exciton diffusion length of organic materials requires that the donor and acceptor materials interpenetrate on a small scale since excitons that are generated far away from the interface will not be able to generate charges before recombination. However, the transport of the separated charges must be ensured as well, and each material must provide a continuous path along which the charges can be readily transported to their respective contacts.

The small geometrical interface of the planar double-layer heterojunction solar cell[5,10] is not optimized for charge generation; however, the created charges are spatially separated and largely confined to the donor and acceptor side of the interface, and charge recombination losses are reduced. The bulk heterojunction consists of an interpenetrating network of donor and acceptor material.[6,11−14] This configuration decreases the distance an exciton must travel to reach an interface, diminishing the loss mechanism of exciton recombination. However, while on transit to the electrodes, charges have the possibility of meeting an opposite charge, resulting in enhanced recombination and reduced current. Carrier mobility in the blend is usually reduced,[7,8,10] and the

* To whom correspondence should be addressed. Phone: +41 44 8234084. Fax: +41 44 8234012. E-mail: roland.hany@empa.ch.
[†] Empa, Swiss Federal Laboratories for Materials Testing and Research.
[‡] Universidade de São Paulo.
[§] UNESP.
[||] Institute of Physics.

(1) Coakley, K. M.; McGehee, M. D. *Chem. Mater.* **2004**, *16*, 4533−4542.
(2) Brabec, C. J. *Sol. Energy Mater. Sol. Cells* **2004**, *83*, 273−292.
(3) Gledhill, S. E.; Scott, B.; Gregg, B. A. *J. Mater. Res.* **2005**, *20*, 3167−3179.
(4) Hoppe, H.; Sariciftci, N. S. *J. Mater. Res.* **2004**, *19*, 1924−1945.
(5) Tang, C. W. *Appl. Phys. Lett.* **1986**, *48*, 183−185.
(6) Li, G.; Shrotriya, V.; Huang, J.; Yao, Y.; Moriarty, T.; Emery, K.; Yang, Y. *Nat. Mater.* **2005**, *4*, 864−868.
(7) Xue, J.; Rand, B. P.; Uchida, S.; Forrest, S. R. *Adv. Mater.* **2005**, *17*, 66−71.
(8) Peumans, P.; Yakimov, A.; Forrest, S. R. *J. Appl. Phys.* **2003**, *93*, 3693−3723.
(9) Snaith, H. J.; Greenham, N. C.; Friend, R. H. *Adv. Mater.* **2004**, *16*, 1640−1645.
(10) Alam, M. M.; Jenekhe, S. A. *Chem. Mater.* **2004**, *16*, 4647−4656.
(11) Yu, G.; Gao, J.; Hummelen, J. C.; Wudl, F.; Heeger, A. J. *Science* **1995**, *270*, 1789−1791.
(12) Halls, J. J. M.; Walsh, C. A.; Greenham, N. C.; Marseglia, E. A.; Friend, R. H.; Moratti, S. C.; Holmes, A. B. *Nature* **1995**, *376*, 498−500.
(13) Watkins, P. K.; Walker, A. B.; Verschoor, G. L. B. *Nano Lett.* **2005**, *5*, 1814−1818.
(14) Kim. Y.; Cook, S.; Tuladhar, S. M.; Choulis, S. A.; Nelson, J.; Durrant, J. R.; Bradley, D. D. C.; Giles, M.; McCulloch, I.; Ha, C.-S.; Ree, M. *Nat. Mater.* **2006**, *5*, 197−203.

10.1021/cm061660r CCC: $33.50
Published on Web 10/07/2006

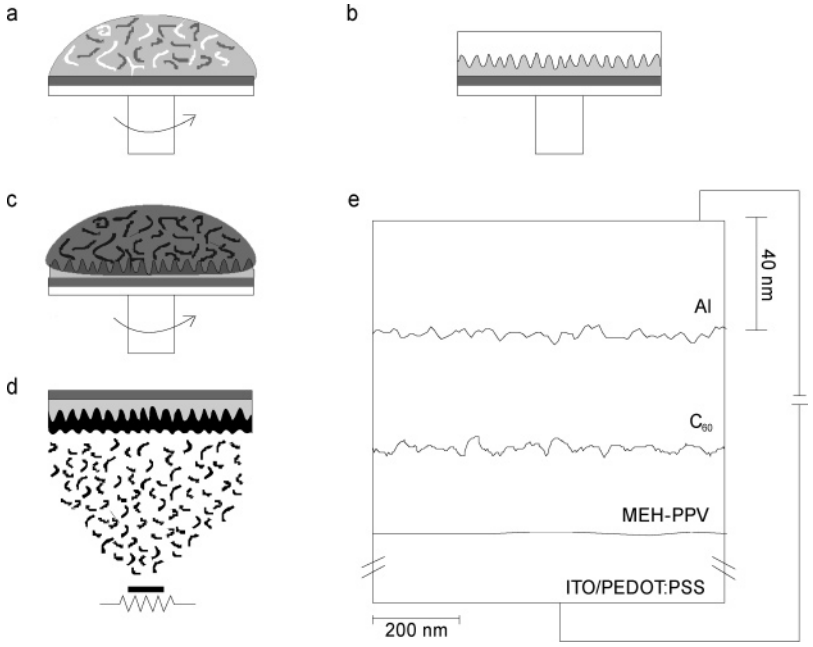

Figure 1. Schematic diagram describing the fabrication process of an interface-enhanced bilayer film, and the final photovoltaic device. (a) An immiscible semiconducting polymer/guest polymer mixture is spin-coated from a common solvent. (b) Polymer demixing during spin coating results in a vertically segregated bilayer thin film with a rough, nanostructured interface. Subsequently, the guest polymer is removed using a selective solvent. The remaining semiconducting polymer is covered with a layer of a second, active component. This can be done either via spin coating (c), again from a selective solvent, or via thermal evaporation (d). (e) Cross section of the actual device structure. The guest polymer was polystyrene, which was selectively removed with the solvent cyclohexane. Interfaces are represented as experimental cross sections from atomic force microscope images.

cell series resistance is high due to the occurrence of charge traps, space charge buildup, and charge recombination at high illumination intensites.[8,9,15] The controlled self-organization at the nanometer scale during and after blend film formation depends strongly on a number of fabrication parameters that need to be optimized for each and every new material combination.[3,4,16] In the best bulk heterojunction devices, a soluble C_{60} derivative (PCBM) has been used with conjugated polymers. For a poly(*p*-phenylenevinylene) derivative, power-conversion efficiencies of 2.5% have been reported,[17] and with use of poly(3-hexylthiophene) as the electron donor, solar cells approaching the 5% efficiency benchmark have been demonstrated.[6,14,18]

Recent efforts in manipulating and controlling the structure of organic thin films tried to combine the high efficiency of charge generation of the bulk heterojunction with the low resistance to charge transport of the planar heterojunction in a single-device configuration. For polymer-based systems, laminated double-layer arrangements, heat-induced interdiffusion, or selective dissolution has been used to create bilayers with highly folded, or intercalated, heterojunctions.[19−21] With use of small organic molecules, device concepts consisting of a mixed layer of donor and acceptor molecules sandwiched between homogeneous layers, such as the controlled growth of a molecular bulk heterojunction using organic vapor-phase deposition, have proven exceptionally successful.[7,15]

Here, we apply the phenomenon of polymer demixing during spin coating to produce nanostructured, semiconducting polymer films and demonstrate their use to produce efficient heterojunction organic solar cells that consist of a large interface area between the donor and acceptor with connecting paths to the respective electrodes for both materials at the same time. A scheme of the fabrication process is shown in Figure 1. Blends of semiconducting polymer and polystyrene (PS) were used to spin coat active thin structured films. Unlike previously[22] where PS was used as an additive, its role in this work is a sacrificial one since after spin coating PS was removed to take advantage of the structured semiconducting film. To verify the concept, we used the archetypal material combination[20,21,23−27] MEH-PPV (poly[2-methoxy-5-(2′-ethylhexyloxy)-1,4-phenylenevinylene]) and C_{60} to produce solar cells in both the planar and structured, interface-enhanced configuration. Structured devices showed white light efficiencies up to 0.64%, and the monochromatic power conversion efficiency reached 2.97% at 480 nm. These values are ∼3 times higher than

(15) Yang, F.; Shtein, M.; Forrest, S. R. *Nat. Mater.* **2005**, *4*, 37−41.
(16) Hoppe, H.; Sariciftci, N. S. *J. Mater. Chem.* **2006**, *16*, 45−61.
(17) Shaheen, S. E.; Brabec, C. J.; Sariciftci, N. S.; Padinger, F.; Fromherz, T.; Hummelen, J. C. *Appl. Phys. Lett.* **2001**, *78*, 841−843.
(18) Ma, W.; Yang, C.; Gong, X.; Lee, K.; Heeger, A. J. *Adv. Funct. Mater.* **2005**, *15*, 1617−1622.
(19) Granström, M.; Petritsch, K.; Arias, A. C.; Lux, A.; Andersson, M. R.; Friend, R. H. *Nature* **1998**, *395*, 257−260.
(20) Drees, M.; Davis, R. M.; Heflin, J. R. *Phys. Rev. B* **2004**, *69*, 165320.
(21) Fujii, A.; Mizukami, H.; Umeda, T.; Shirakawa, T.; Hashimoto, Y.; Yoshino, K. *Jpn. J. Appl. Phys.* **2004**, *43*, 8312−8315.
(22) Brabec, C. J.; Padinger, F.; Hummelen, J. C.; Janssen, R. A. J.; Sariciftci, N. S. *Synth. Met.* **1999**, *102*, 861−864.
(23) Krebs, F. C.; Carlé, J. E.; Cruys-Bagger, N.; Andersen, M.; Lilliedal, M. R.; Hammond, M. A.; Hvidt, S. *Sol. Energy Mater. Sol. Cells* **2005**, *86*, 499−516.
(24) Davenas, J.; Alcouffe, P.; Ltaief, A.; Bouazizi, A. *Macromol. Symp.* **2006**, *233*, 203−209.
(25) Sariciftci, N. S.; Braun, D.; Zhang, C.; Srdanov, V. I.; Heeger, A. J.; Stucky, G.; Wudl, F. *Appl. Phys. Lett.* **1993**, *62*, 585−587.
(26) Gao, J.; Hide, F.; Wang, H. *Synth. Met.* **1997**, *84*, 979−980.
(27) Hayashi, Y.; Yamada, I.; Takagi, S.; Takasu, A.; Soga, T.; Jimbo, T. *Jpn. J. Appl. Phys.* **2005**, *44*, 1296−1300.

results for planar devices and the highest efficiencies reported for that material combination so far, including bulk heterojunctions.

Experimental Section

Photovoltaic devices were fabricated in a sandwich structure between indium tin oxide (ITO, anode) and aluminum (cathode). ITO-coated glass substrates (Merck, sheet resistance 30 Ω square^{-1}) were cleaned in a laminar flow hood by successive ultrasonic treatment in acetone, ethanol, detergent (Hellma), and Milli-Q water. A 80 nm thick layer of poly(ethylene dioxythiophene) doped with polystyrene sulfonic acid (PEDOT:PSS, Bayer) was spin-coated on top of ITO. After being heated on a hot plate for 1 h at 120 °C under vacuum, the substrates were transferred to a nitrogen-filled glovebox (<1 ppm O_2 and H_2O). Poly[2-methoxy-5-(2′-ethylhexyloxy)-1,4-phenylene-vinylene] (MEH-PPV, M_n = 40 000−70 000, Aldrich) was purified by dissolving in THF (1 g 100 mL^{-1}), followed by filtration, precipitation in a tenfold excess of methanol, and drying in a vacuum oven at 65 °C. Stock solutions of MEH-PPV (5 mg mL^{-1}) and polystyrene (10 mg mL^{-1}, PS, GPC standards from Fluka with molecular weights of 3000 and 70 000, denoted as PS3 and PS70, respectively) were prepared in chloroform (CF) and chlorobenzene (CB). For planar bilayer devices, a MEH-PPV film with a thickness of typically 30 nm (measured with a profilometer from Atomic Force) was spin-coated from CB onto PEDOT:PSS. Blended films were prepared by mixing together different quantities of MEH-PPV and PS stock solutions before spin coating. If necessary, the blend solution was diluted to adjust the final MEH-PPV film thickness to ∼30 nm. PS was then removed by dipping the substrate for 1 min into cyclohexane. Devices were kept in high vacuum (∼9 × 10^{-7} mbar) for at least 2 h prior to the sublimation of a 40 nm thick layer of C_{60} (99.95% purity, SES Research). Then, 40 nm of Al was thermally evaporated as the top contact, providing devices with active areas of 7.1 or 3.2 mm^2, respectively. Substrates were rotated (2 rpm) for the deposition of C_{60} and Al.

A homemade airtight transfer box was used to keep the devices under N_2 during characterization. The quantum efficiency as a function of wavelength was measured with a 300 W xenon lamp in combination with a Cornerstone 130 monochromator (Oriel). The light spot area was 12.6 mm^2 and the number of photons for each wavelength was calculated by using a calibrated Si diode as reference. Internal photon-to-electron conversion (IPCE) values were calculated as IPCE = 1240 × J × λ^{-1} × P_{in}^{-1}, where J (A cm^{-2}) is the measured photocurrent density and P_{in} (W cm^{-2}) is the incident light power at each wavelength λ (nm). Current vs voltage curves were recorded with a Keithley 2400 source/measure unit in the dark and under white light irradiation using the full Xe lamp spectrum and an AM1.5G filter set with a power density of 56.6 mW cm^{-2} (measured with a thermopile power meter, Oriel). Power efficiencies were calculated as η = FF × J_{sc} × V_{oc} × P_{in}^{-1}, where J_{sc} (A cm^{-2}) is the short-circuit current, V_{oc} (V) is the open-circuit voltage, FF = V_m × J_m × V_{oc}^{-1} × J_{sc}^{-1} is the fill factor, and V_m and J_m are current and voltage for maximum power output. No corrections were made for losses due to absorption and reflection of incident light illumination at the glass/ITO/polymer interfaces.

Atomic force microscopy (AFM) measurements were performed on a Digital Instruments Multimode Scanning Microscope (Nanoscope III) in tapping mode using etched silicon probes with tip radii of ∼10 nm. For experimental convenience, mica (1 cm × 1 cm) was used as a substrate, on which a 80 nm thick PEDOT:PSS layer was spin-coated. For accurate comparison, the film preparation conditions for AFM measurements were kept the same as those for the photovoltaic devices. Dissolution of PS from blended films was investigated with a UV−vis spectrophotometer (Varian Cary 50). The absorption spectrum of a 80 nm thick PEDOT:PSS layer spin-coated on quartz glass was the baseline for these measurements, and the spectrum of a single layer of MEH-PPV on PEDOT:PSS/quartz was used as the reference. Blend solutions of MEH-PPV and PS were then spin-coated on the same substrate, and films were kept in cyclohexane for different periods. The decrease of the absorption in the 200−250 nm range was used to follow the dissolution of PS, and the constant absorbance in the 400−600 nm range showed that MEH-PPV was not affected by cyclohexane. Fluorescence measurements were performed on a Fluorolog-3 spectrofluorometer (Jobin Yvon Horiba) in front-face detection mode.

Results and Discussion

Thin films (∼30 nm) of MEH-PPV were prepared on PEDOT:PSS-coated (∼80 nm) ITO glass substrates. Structured layers were prepared by spin coating blends of MEH-PPV and polystyrene (PS), dissolved in chlorobenzene (CB), chloroform (CF), or mixtures of CB and CF. After spin coating, PS was removed with the selective solvent cyclohexane. We used PS with different molecular weights (M_n = 3000 and 70 000, denoted as PS3 and PS70, respectively), different blend ratios and solvent mixtures to study the surface-directed polymer demixing process, with the aim to obtain MEH-PPV topographical structures with dimensions of the exciton diffusion lengths for both materials (7−40 nm).[8,10,28] Approximately 40 nm thick layers of C_{60} and Al were subsequently evaporated on MEH-PPV, to yield device structures such as the one shown in Figure 1.

Spin coating the MEH-PPV/PS polymer blend in a controlled manner is the central aspect for the successful realization of this device configuration. Mixtures of polymers deposited from a common solvent tend to phase separate during evaporation of the solvent. However, during spin coating the solvent evaporates quickly, and the demixing is not complete. The domain sizes of the three-dimensional morphology and surface topography of the film can be controlled by varying parameters such as solvent,[29] polymer size,[30] concentration,[31] and the rate of evaporation.[32] In contrast to polymer demixing in the bulk, the substrate also has a strong influence on the morphology,[33] and surface-oriented phase separation can be induced, which leads to wetting layers of either of the two components.[29,33]

Figure 2 shows selected AFM images and cross sections of patterned MEH-PPV films after PS removal. Films were spin-coated on PEDOT:PSS and thus developed the same morphology as in the actual device fabrication process. We observed a strong demixing of the two phases during spin

(28) Markov, D. E.; Tanase, C.; Blom, P. W. M.; Wildeman, J. *Phys. Rev. B* **2005**, *72*, 045217.
(29) Arias, A. C.; Corcoran, N.; Banach, M.; Friend, R. H.; MacKenzie, J. D.; Huck, W. T. S. *Appl. Phys. Lett.* **2002**, *80*, 1695−1697.
(30) Snaith, H. J.; Friend, R. H. *Thin Solid Films* **2004**, *451−452*, 567−571.
(31) Iyengar, N. A.; Harrison, B.; Duran, R. S.; Schanze, K. S.; Reynolds, J. R. *Macromolecules* **2003**, *36*, 8978−8985.
(32) Halls, J. J. M.; Arias, A. C.; MacKenzie, J. D.; Wu, W.; Inbasekaran, M.; Woo, E. P.; Friend, R. H. *Adv. Mater.* **2000**, *12*, 498−502.
(33) Walheim, S.; Böltau, M.; Mlynek, J.; Krausch, G.; Steiner, U. *Macromolecules* **1997**, *30*, 4995−5003.

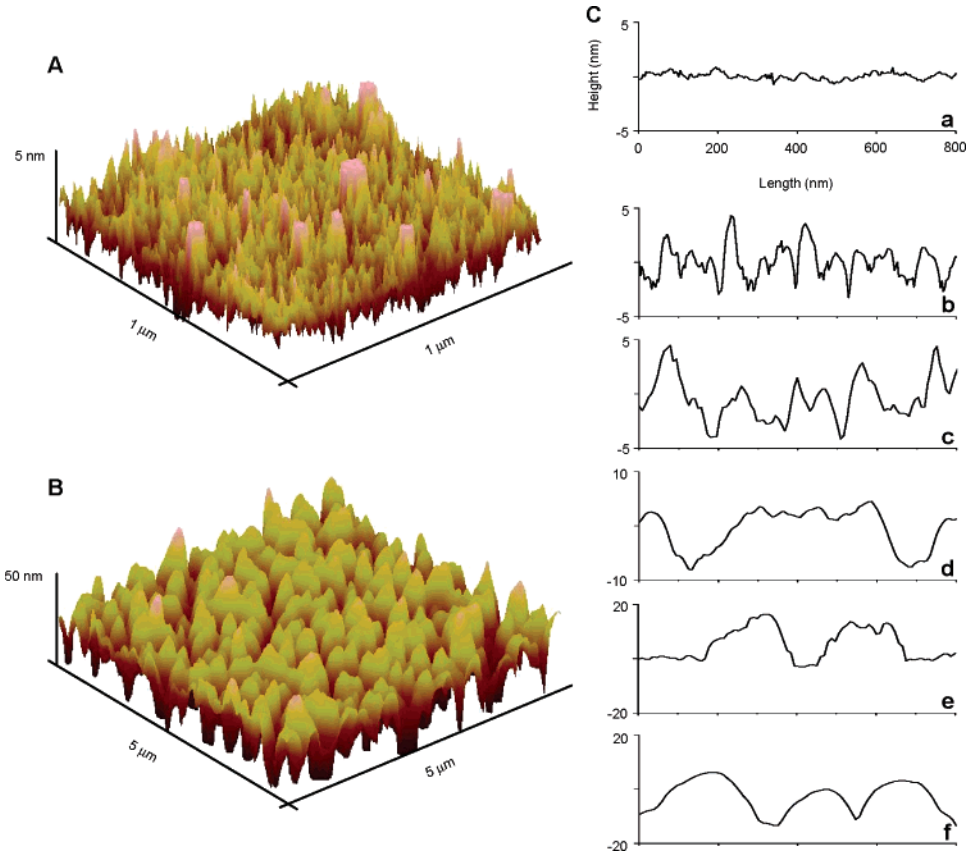

Figure 2. Atomic force microscope (AFM) images and cross sections of spin-coated thin films after polystyrene (PS) removal. (A) 3D height image from a MEH-PPV/PS (M_n = 3000, denoted as PS3) blend (1:2 w/w) dissolved in chlorobenzene (CB):chloroform (CF) (1:1 v/v). (B) 3D height image from a MEH-PPV/PS (M_n = 70 000, denoted as PS70) blend (1:2 w/w) in CB:CF (1:1 v/v). (C) Cross sections of AFM height images from a (a) MEH-PPV-only film, (b) MEH-PPV/PS3 blend (1:2 w/w) in CB, (c) MEH-PPV/PS3 blend (1:2 w/w) in CB:CF (1:1 v/v), (d) MEH-PPV/PS3 blend (1:2 w/w) in CF, (e) MEH-PPV/PS3 blend (1:4 w/w) in CB:CF (1:1 v/v), (f) MEH-PPV/PS70 blend (1:2 w/w) in CB. Average maximum heights of the profiles were R_z = 2.3, 3.1, 6.3, 7.3, and 28 nm for images C(b)−C(f).

coating and a preferential aggregation of the more polar MEH-PPV at the surface. A film spin-coated from single MEH-PPV is almost planar (Figure 2C(a)), but PS induced a significant increase of the polymer−polymer interface roughness with characteristic topographical variations left in the MEH-PPV films. For identical polymer ratios and solvents (Figure 2A vs 2B, Figure 2C(b) vs 2C(f)), PS70 resulted in more pronounced topographical undulations with lateral length scales of ∼200 nm and thickness variations of ∼10−30 nm, whereas the surfaces using PS3 appeared smoother with irregular height fluctuations of ∼5 nm. This can be explained with the less favored demixing using higher molecular-weight polymers.[30] The roughness dimensions of the interface topography increased also for increasing PS contents, illustrated when spin coating a blend of 20% MEH-PPV with a high fraction of 80% PS3 (Figure 2C(e)). When the solvent is changed from CB to CF, the serrated surface (Figure 2C(b)) changed to a topography with distinct craters (Figure 2C(d)). These films were spin-coated with PS3, but the same trend was observed for PS70. With use of a 50% CB to 50% CF solvent mixture for PS70 (Figure 2B), spin coating resulted actually in deep holes with dimensions (∼30 nm) of the film thickness. This indicates a pointwise lateral demixing that did not occur when CB was used as the single solvent (Figure 2C(f)). Comparable AFM images were obtained after storage in the glovebox for several weeks, indicating the stability of topographical features in these structured thin films.

These experimental findings seem to agree with the model of the polymer demixing process recently developed by Heriot and Jones.[34] The initial phase separation takes place in a surface-oriented fashion forming a transient bilayer, followed by the potential breakup of the layers because of interfacial instability. It was suggested that the instability arises because of a solvent-concentration gradient through the film, which will be more pronounced for fast evaporating solvents (such as CF). Figures 2B and 2C(d) can then be interpreted as the early stages of the lateral demixing process. For a slowly evaporating solvent (such as CB), solvent diffusion will be able to maintain a spatially uniform solvent concentration, removing the driving force for interface instability. Therefore, the topographies in Figures 2C(b,f) appear smoother with probably random height variations. Finally, Figure 2C(c) illustrates the intermediate stage when using a 50% CB to 50% CF solvent mixture.

Lateral demixing is undesired for efficient photovoltaic devices. This is because covering of the second active organic layer will then contact both electrodes at the same time. These direct paths between cathode and anode act as a shunt resistance in parallel with the active part of the device,

(34) Heriot, S. Y.; Jones, R. A. L. *Nat. Mater.* **2005**, *4*, 782−786.

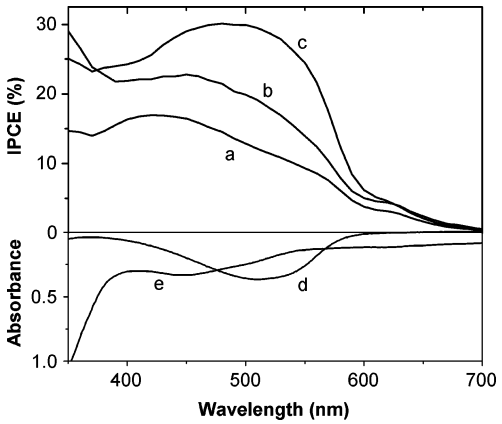

Figure 3. Internal photon-to-electron conversion (IPCE) efficiencies and absorbance spectra of thin films. Upper part, IPCE spectra of ITO/PEDOT:PPS/MEH-PPV/C_{60}/Al devices for a (a) planar MEH-PPV layer, (b) structured layer from a MEH-PPV/PS70 (1:2 w/w) blend in CB, and (c) structured layer from a MEH-PPV/PS3 (1:2 w/w) blend in CB. Lower part, absorption spectra of thin films (d) of MEH-PPV and (e) of C_{60}.

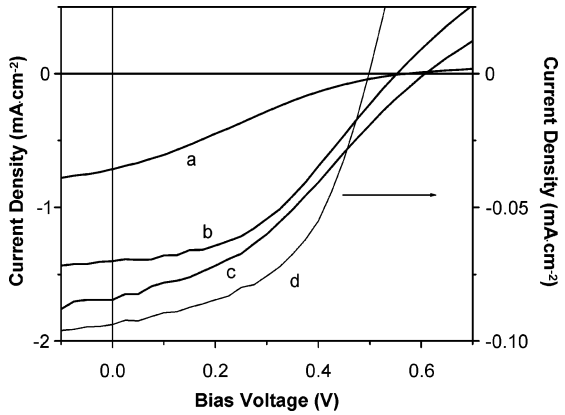

Figure 4. Current density vs voltage (J vs V) of photovoltaic devices under white light and monochromatic (480 nm) light illumination. Left, J vs V characteristics of ITO/PEDOT:PPS/MEH-PPV/C_{60}/Al devices under white light excitation (56.6 mW cm^{-2}). (a) Planar MEH-PPV layer, (b) structured layer from a MEH-PPV/PS70 (1:2 w/w) blend in CB, (c) structured layer from a MEH-PPV/PS3 (1:2 w/w) blend in CB. Right, (d) J vs V characteristics of a structured device from a MEH-PPV/PS3 (1:2 w/w) blend in CB and excited at 480 nm (0.8 mW cm^{-2}). Devices showed dark currents below 10^{-7} A cm^{-2} and rectification factors at $\pm$0.8 V of $\sim$90 for the planar layer and $\sim$670 for the structured devices.

resulting in a lowering of the open-circuit voltage.[9] Devices were therefore fabricated using structured MEH-PPV layers as shown for example in Figures 2C(b,f). The internal photon-to-current conversion (IPCE) spectra are summarized in Figure 3. Compared to the planar bilayer device, structuring resulted in a photocurrent increase and reached a remarkable maximum value of $\sim$30% in the 480−500 nm range. The increase is more pronounced in the region of MEH-PPV absorption (450−550 nm) than at wavelengths where predominantly C_{60} is excited (<450, $\sim$600 nm), and larger when using the topographical MEH-PPV surface shown in Figure 2C(b). This can be explained with the different exciton diffusion lengths of MEH-PPV ($\sim$10 nm[8,10,28]) and C_{60} ($\sim$40 nm[8]). The small-scale structured surface resulted in a higher relative increase of the donor−acceptor interface that lies within the diffusion length of MEH-PPV than the undulated topography with lateral dimensions of $\sim$200 nm (Figure 2C(f)). The IPCE values for wavelengths below 400 nm indicate that both structured MEH-PPV layers increased the charge-transfer efficiency after C_{60} photoexcitation to a similar extent.

The merits of the IPCE data are reflected in the device performances under white light illumination (Figure 4, Table 1). The short-circuit current densities (J_{sc}) of structured devices are about twice that obtained for the planar bilayer configuration. At the same time, the open-circuit voltages (V_{oc}) remained high, which is essential for achieving high electrical power output. Included in Table 1 are device performance data from the literature. Due to different material purities and experimental techniques used, a detailed result comparison between different laboratories is certainly not meaningful.[3] However, the data serve to illustrate that the performance figures obtained using structured devices, such as power efficiencies of η = 0.64% and 2.97% for white light and monochromatic illumination, are much better than what has been achieved so far.

Increased charge generation in structured layers is corroborated by photoluminescence (PL) quenching (Figure 5). For the MEH-PPV/C_{60} material combination the photoinduced electron transfer is more than 10^3 times faster than the radiative or nonradiative exciton decay, and the efficiency for charge separation within the exciton diffusion length is close to unity.[11,25,26] Compared with a single layer of MEH-PPV, relative values of 35% and 7% PL efficiencies were

Table 1. Comparison of Device Performance of MEH-PPV/C_{60} Photovoltaic Devices

	$\lvert J_{sc}\rvert$[a] (mA cm^{-2})	V_{oc} (V)	FF (%)	η (%)	ref
White Light					
planar double layer[b]	0.71	0.57	22.6	0.16	this work
structured, PS (M_n = 70 000)[b]	1.40	0.55	42.5	0.58	this work
structured, PS (M_n = 3000)[b]	1.69	0.61	35.1	0.64	this work
100 mW cm^{-2}	0.57	0.54		0.20	27
100 mW cm^{-2}	0.50	0.65	26.7	0.09	23
Monochromatic Light					
planar double layer, 480 nm, 0.8 mW cm^{-2}	0.044	0.46	45.6	1.15	this work
structured, PS (M_n = 3000), 480 nm, 0.8 mW cm^{-2}	0.094	0.50	50.6	2.97	this work
500 nm, 0.3 mW cm^{-2}	0.035	0.44	19	0.98	21
514.5 nm, 1 mW cm^{-2}	0.002	0.44	23	0.02	25
470 nm, 3.8 mW cm^{-2}	0.092	0.50	25	0.30	20

[a] J_{sc} is the short-circuit current density, V_{oc} the open-circuit voltage, FF the fill factor, and η the external power efficiency. [b] The illumination intensity was 56.6 mW cm^{-2}.

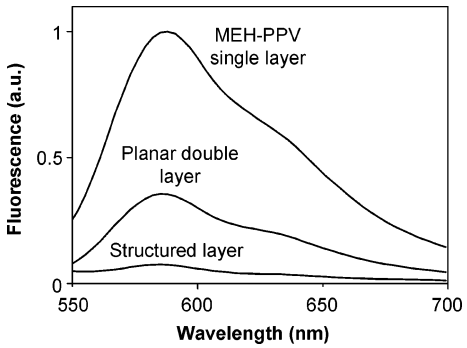

Figure 5. Fluorescence spectra of MEH-PPV and MEH-PPV/C_{60} (40 nm) films. Spectra were normalized by the amount of absorbed light at the excitation wavelength of 530 nm. The structured MEH-PPV layer was spin-coated from a mixture with PS3 (1:2 w/w) from CB. The MEH-PPV emission in the planar bilayer configuration was quenched by about 60% and in the structured device by more than 90%.

measured for planar and structured layers using C_{60}. This substantial increase in PL quenching indicates that indeed the rough MEH-PPV/C_{60} interface, allowing for more charge generation, is directly connected to the efficiency improvement in structured devices. However, only an apparently much larger exciton diffusion length than the known value of ~10 nm for MEH-PPV would explain the almost complete PL quenching in a 30 nm thick structured polymer layer as shown in Figure 1e.[10,35] We argue that this pronounced PL decrease is due to intermixing of the evaporated C_{60} with MEH-PPV. It has been demonstrated that C_{60} diffuses into spin-coated PPV-based polymer films on a time scale of several hours,[35] leading to an extended zone in the polymer layer where PL quenching and charge generation occurs. The thickness of this C_{60}/MEH-PPV intermixed region is larger for the structured layers, which we suspect to be the signature of the demixing process with entangled MEH-PPV and PS chains forming a diffuse interface. PS removal then results in a MEH-PPV surface containing pinholes with small-scale dimensions that allow C_{60} to penetrate easily into the polymer layer during the evaporation process or by subsequent diffusion.

The intermixed zone not only increased charge generation but also effectively reduced the device-limiting hole charge-transport distances to the anode and allowed for more efficient charge collection. This is reflected in a rise of the fill factors (FF) from ~23% to >35% for white light illumination (Table 1). A rise of FF indicates a smaller series resistance and is attributed to more effective charge transport.[4] Normalizing the curves of Figure 5 to the same maximum value showed identical spectra for the red portion of the PL. Enhanced emission at higher wavelengths would indicate a higher degree of MEH-PPV interchain aggregation in the films spin-coated from MEH-PPV/PS mixtures, which in turn enhances the mobility of carriers.[36,37] We can therefore rule out this other possibility that enhanced mobility of charge carriers in the structured layer is the reason for the rise of FF in these devices.

As apparent from Figure 1e, the C_{60} top surface conforms to the underlying interface, resulting in a second, folded C_{60}/Al interface. Increased electrode roughness can lead to electric field-enhancing properties of tiplike structures, which affect both the carrier transport and injection.[38,39] In addition, more undulating surfaces with larger dimensions might effectively increase the light absorbed within the active layer since the optical path length is increased for light reflected at angles other than normal to incident. These mechanisms, related to the nonplanar geometry of the reflecting back electrode, can in our devices only account for minor efficiency improvements at most (Supporting Information).

Conclusion

The substantial freedom in the choice of the guest polymer and the sequential deposition of donor/guest and acceptor materials offers a great flexibility to control the polymer-based self-organization process and to optimize the local phase separation and nanoscale morphology of the donor−acceptor interface. In addition, the two-step concept allows for the independent design of a desired layer topography that can be covered with a series of second active components. This is in contrast to the direct spin coating of a donor−acceptor polymer blend mixture, where the desired morphology has to be re-adjusted for every new materials combination.[16] More significantly, the method results in device performance increase for materials combination where the development of an effective bulk heterojunction is hindered. This is especially true for the fullerene used here since the limited solubility of C_{60} and its tendency toward crystallization and aggregation during film formation limits its use in high-concentration blends.[11,20,24] Further work will involve the extension of the concept where also the second active component will be applied via spin coating.

Supporting Information Available: Absorbance spectra of MEH-PPV and MEH-PPV/PS films before and after PS removal; absorbance spectra and total organic layer thickness of photovoltaic devices; evaluation of electric field effects induced by the rough cathode interface. This material is available free of charge via the Internet at http://pubs.acs.org.

CM061660R

(35) Markov, D. E.; Amsterdam, E.; Blom, P. W. M.; Sieval, A. B.; Hummelen, J. C. *J. Phys. Chem. A* **2005**, *109*, 5266−5274.
(36) Nguyen, T.-Q.; Martini, I. B.; Liu, J.; Schwartz, B. J. *J. Phys. Chem. B* **2000**, *104*, 237−255.
(37) Geens, W.; Shaheen, S. E.; Wessling, B.; Brabec, C. J.; Poortmans, J.; Sariciftci, N. S. *Org. Electron.* **2002**, *3*, 105−110.
(38) Novikov, S. V. *Macromol. Symp.* **2004**, *212*, 191−200.
(39) Tutis, E.; Berner, D.; Zuppiroli, L. *Proc. SPIE* **2004**, *5464*, 330−336.